

# Scalable Quantum Networks: Congestion-Free Hierarchical Entanglement Routing with Error Correction

Hyeonrak Choi,<sup>1,\*</sup> Marc G. Davis,<sup>1</sup> Álvaro G. Iñesta,<sup>2</sup> and Dirk R. Englund<sup>1,†</sup>

<sup>1</sup>Research Laboratory of Electronics, Massachusetts Institute of Technology, Cambridge, Massachusetts 02139, USA

<sup>2</sup>QuTech, Delft University of Technology, Lorentzweg 1, 2628 CJ Delft, The Netherlands

(Dated: June 16, 2023)

We propose quantum tree networks for hierarchical multi-flow entanglement routing. The end nodes on the leaves of the tree communicate through the routers at internal nodes. In a  $k$ -ary tree network, each node is connected to  $k$  nodes in the lower layer, and the channel length connecting two nodes grows with rate  $a_k$  as we move from the leaf to the root node. This architecture enables the qubit-per-node overhead for congestion-free and error-corrected operations to be sublinear in the number of end nodes,  $N$ . The overhead scaling for  $k$ -ary tree is  $\mathcal{O}(N^{\log_k a_k} \cdot \log_k N)$ . Specifically, the square-lattice distributed end nodes with the quaternary tree routing leads to an overhead  $\sim \mathcal{O}(\sqrt{N} \cdot \log_4 N)$ . For a minimal surface-covering tree, the overhead  $\sim \mathcal{O}(N^{0.25} \cdot \log_4 N)$  for  $k = 4$  and is sublinear for all  $k$ . We performed network simulations of quantum tree networks that exhibits size-independent threshold behavior. The routing in tree network does not require time-consuming multi-path finding algorithms. These properties satisfy the essential requirements for scalable quantum networks.

## I. INTRODUCTION

Quantum networks (QNs) present a solution to the challenge of transmitting quantum states across space, time, and physical modalities, in the field of quantum information science and technology [1]. QNs entangle remote quantum memories via optical channels to enable applications such as communication, resource sharing [2], blind quantum computing [3], and distributed sensing [4]. A central research goal focuses on developing architectures and algorithms for *entanglement routing*, which consists of distributing entanglement states among multiple end nodes with high fidelity and rate [5–8].

Photonic channels enable long-distance entanglement due to fast signal propagation, low loss of 0.14 dB/km [9], and negligible thermal noise at room temperature [10]. Optically heralded entanglement generation maps channel losses into reduced entanglement generation rates without lowering fidelities [11]. However, photon-based schemes encounter a significant challenge in long-distance transmission due to the exponential decay of photon transmission. Consequently, the development of quantum repeaters becomes imperative to mitigate photon losses and ensure high generation rates [12]. Moreover, within the network, quantum repeaters play an additional role as routers, efficiently distributing entanglements to nodes that are not directly connected [7].

To distribute entanglement to two dedicated end nodes, QNs generate short-distance entanglement and perform entanglement swapping over the path connecting the two. The intermediate nodes need to perform the following tasks:

1. Perform a repeat-until-success procedure of heralded entanglement generation [13, 14].
2. Maintain quantum states in memories until receiving a classical signal of successful entanglement generation.
3. Select two qubits entangled with different nodes and perform Bell measurements for entanglement swapping [12].
4. Restore fidelities diminished by imperfect operations entanglement using purification [15] or quantum error correction [16, 17].

The processes require two-way classical communications, particularly for probabilistic results such as entanglement heralding and purification. During this delay, the quantum network either reserves a path or dynamically searches for the path for a pair of end nodes. Thus, the network operation is close to the circuit-switched network [18], where the channel usage of one party blocks the use by others.

In addition, current and near-future technologies for quantum networks are *memory-limited*; The number of memories is many orders of magnitude smaller than the capacity of optical channels. The state-of-the-art demonstration has shown the use of four memories [19], and even the largest quantum computer without networking capabilities has 433 qubits (IBM Osprey) [20]. On the other hand, optical channels can transmit millions of single photons within the coherence time of these memories [21]. This is a crucial difference from classical networks, where large memory volumes are accessible, and communication is constrained by channel capacity (*channel-limited* system).

In a memory-limited network, circuit switching can lead to congestion, which occurs when the number of entanglement routing paths trying to access a router simultaneously exceeds the number of available qubits in the router. However, in order to justify the implementation of a large-scale quantum network, it is necessary to

\* choihr@mit.edu

† englund@mit.edu

ensure that the network is capable of handling a significant number of entanglement routings. A trivial solution is to linearly increase the number of memories in routers. Thus, the central question is: *how many qubits are minimum for multiflow entanglement routing across many end nodes?*

“Scalable” quantum networks should support simultaneous multi-flow entanglement routing, the number of which scales with the size of the network, which we define as the number of end nodes. This is equivalent to linearly increasing aggregated network capacity and constant throughput. We need to prevent the accumulation of operational errors for reliable entanglement sharing with quantum error correction. Furthermore, routers should be sufficiently buffered so that the network is congestion-free. It is trivial to achieve those with a linearly increasing number of qubits per user, which we define as overhead. However, it is too expensive. We desire a sublinear overhead with network effects.

**Definition 1.** *An  $N$ -user quantum network is scalable if the network allows:*

*Condition 1:  $\mathcal{O}(N)$  error-corrected entanglement flow*

*Condition 2: without congestion*

*Condition 3: with  $o(N)$  quantum memories*

*Assumption: for uniform random traffic.*

Note that the conditions depend on the network model. Here, we assume a uniform random traffic model in which every end node requests entanglement with every other end node with equal probability, but the gross probability that one node engages in entanglement is assumed to be fixed (Assumption). This results in the average number of multi-flow entanglements to be linearly increasing with the number of network end nodes (Condition 1). A network is ‘congestion-free’ if the routing paths of multi-flow entanglement requests do not exceed the number of memory at any nodes. Formally, we consider a set of requests in a snapshot of networks, that is, a member of the typical set determined by the traffic model. In this limit, the probability of routing failure exhibits exponential decay as the network size increases (Condition 2). The number of memories per end node is required to be sublinear in a scalable network (condition 3).

In this work, we propose a ‘quantum tree network’ (QTN) that meets all the conditions as a scalable network design. A QTN only allows for optimal entanglement routing, enabling fast communication and excluding time-consuming multipath-finding algorithms. We find that the overhead of QTNs can be decomposed into contributions from the repeating-routing and the error correction. If the channel is dominated by insertion loss, the overhead is logarithmic. In the propagation loss dominant regime, the overhead depends on the geometric deployment of the network. If the network grows by adding more end nodes in a fixed area, the overhead remains logarithmic. If the geometric length of the network grows slower than the degree of the tree, the overhead is guaranteed to be sublinear. Specifically for general 2D sur-

face covering, the overhead has sub-square-root end-node scaling.

## II. QUANTUM NETWORK TOPOLOGY

The arrangement of the network resources such as nodes and edges defines a network topology and highly affects the performance of a classical network. A broad range of topologies has been studied and deployed. These topologies span from simple configurations like ring, mesh, bus, and star topologies, to complex data processing structures, such as Clos networks, Omega networks, and fat trees. However, the discussion of quantum network topology has been mostly limited to the 1D repeater chain [22], the star topology [23], and the two-dimensional uniform lattices [7, 8, 24].

Although lattice-based quantum mesh networks are robust under local failures and enable distance-independent communication rates [7, 8, 24], memory congestion prevents them from being scalable. Figure 1(a) shows a square-lattice quantum mesh network. Each node represented by a circle is an end node requesting entanglement. The edges are physical channels through which entanglement is generated. Because every node is only connected to a few neighbors, entanglement should be routed with entanglement swapping. Thus, in a mesh network, each node is a router as well as an end node. Assume that two pairs of end nodes, A-B (light green) and C-D (dark green), request entanglement. The network routes entanglement through one of the shortest paths. If each node has only two qubits, each node can perform only one entanglement swapping at a time. When two routing paths of the requests cross, the network is under congestion.

What is the total number of qubits for multi-flow routing in quantum mesh network? Under uniform random traffic,  $N_e$  entanglement paths over mesh networks have  $\mathcal{O}(N_e^2)$  node intersections (see Appendix A). For  $N_e \sim \mathcal{O}(N)$ , the total number of qubits required is  $\mathcal{O}(N^2)$ . The overhead, the number of qubits per user, is  $\mathcal{O}(N)$  in the congestion-free limit. Note that the actual number of qubits used is  $\mathcal{O}(N\sqrt{N})$  because the average length of routing paths is  $\mathcal{O}(\sqrt{N})$ . One does not know where congestion occurs a priori. Thus, all nodes that can be potentially under congestion should be equipped with qubits capable of maximum traffic, though in most instances they are not (see Appendix A). Another way to avoid congestion is multipath optimization with global information from a network. We assume that this is not available due to computational complexities and finite coherence time (see Appendix F for detailed discussion).

## III. QUANTUM TREE NETWORK

We propose a quantum tree network (QTN) as a scalable quantum network architecture. The QTN architecture employs hierarchical aggregation of routing paths

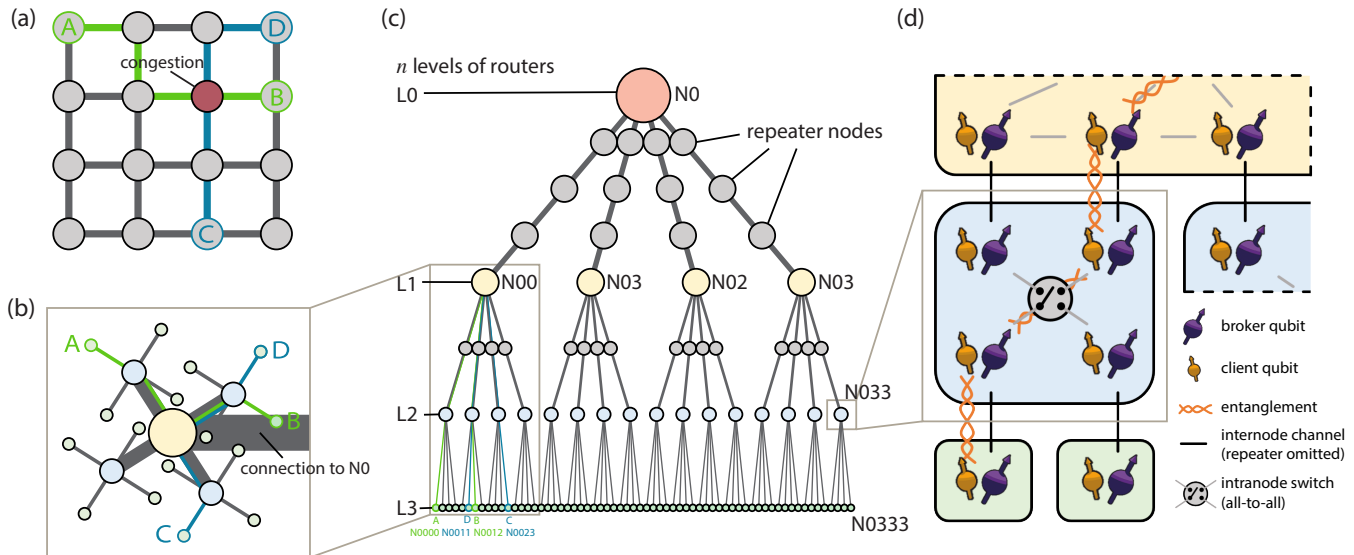


FIG. 1. Congestion-free Tree Network. (a) Quantum mesh network with nodes on a square lattice. The light and dark green lines are the routing paths for A-B and C-D pairs. The red node is on both paths and is congested. (b) Quantum tree network. The size of the nodes is proportional to the number of qubits, and the width of the edges is proportional to the qubit pairs allocated. (c) The hierarchical view of  $k = 4$ -ary quantum tree network. (d) Quantum router architecture.

through routers with a corresponding number of qubits. A similar classical network architecture, the fat tree network, is used in the data centers, where stable throughput is required for random traffic under memory constraint [25]. Ref. [26] showed the scalability and out-performance of classical fat trees compared to other hierarchical designs.

Figure 1(b) describes the entanglement routing for the A-B and C-D pairs. The router where two paths intersect has more qubits as illustrated by a larger node to avoid congestion. In the QTN framework, end nodes do not route entanglement. Instead, we employ dedicated routers to route entanglement flows from end nodes and lower-level routers.

Figure 1(c) details the hierarchical structure of QTN. For a  $k$ -ary tree and  $N$  end nodes, the depth of the tree is  $n = \log_k N$ . The layers with depth- $i$  nodes are labeled  $L_i$ ,  $i \in \{0, 1, \dots, n\}$ . All the nodes but the root and leaves are physically connected to  $k$  other nodes in  $L(i+1)$  and one node in  $L(i-1)$ . The nodes are labeled with “N” followed by  $k$ -ary number, labeling a  $x_j^{\text{th}}$  child attached to the parent  $Nx_0x_1\dots x_{j-1}$  as  $Nx_0x_1\dots x_{j-1}x_j$ . For example, we show A and B in N0000 and N0012. Because they are in different branches of N00, they need entanglement swapping through nodes N000, N00, N001, and N012. Because the tree graph is free of cycles, there is a unique selection of quantum routers for a pair of end nodes. We exemplify our discussion with uniformly branching trees, but our discussion holds for other trees.

Using the notation, Appendix B derived that routers in an upper layer need to route exponentially more entanglement as  $\sim k^{(n-i)}$ . Thus, routers in a higher layer

should have exponentially more qubits to avoid congestion. Furthermore, the nodes can be buffered  $m$  times for faster entanglement generation. All in all, a router in the  $L_i$  layer has  $2mk^{(n-i)}$  qubits with a factor of 2 for the entanglement swapping.

While the architecture described determines the routing, we need to detail the deployment of the QTN nodes because the distances between the router nodes translate to the number of repeaters and ultimately to the resource overhead. For this, we use the growth rate  $a_k$ , the ratio of the distance between a router in  $L_i$  and in  $L(i+1)$  to the one between  $L(i-1)$  and  $L_i$ . An interesting choice of  $a_k$  is the deployment of QTN for minimal 2D surface coverage. Appendix C shows that this construction gives  $a_k < \sqrt{k}$ , and it also details how the router nodes can be deployed to cover nonuniform demands. Another choice of  $a_4^{\text{sq}} = 2$  is for the end nodes distributed on a square lattice. The channel length between  $L_i$  and  $L(i-1)$  is  $\sim a_k^{(n-i)}$ , and the number of repeater stations is proportional to the channel length. A repeater between  $L_i$  and  $L(i-1)$  has  $2mk^{(n-i)}$  qubits to keep the generation rate proportional to the number of qubits in the nodes.

Figure 1(d) illustrates the “quantum router architecture” proposed in ref. [27] ( $m = 1$  for visual clarity). We use broker-client qubits for a robust and scalable entanglement distribution [24, 28]. Broker qubits (purple) in a node generate a heralded entanglement (orange) through the intranode (gray) and internode (black) channels. If the entanglement is heralded, it is stored in client qubits (yellow) with a longer storage time and subsequent entanglement generation. We assume all-to-all intranode connectivities that can possibly be implemented with

trapped-ion systems [29, 30] or color centers in diamond with integrated photonics [31] or spatial light modulators [32]. We assume that the intranode photon loss is negligible compared to the internode and ignore the temporal resources for the intranode routing.

#### IV. RESOURCE OVERHEAD CALCULATION

Here, we analyze the resource overhead of the deployed quantum tree network. We start with a raw entanglement generation rate of each end node,  $R = p_e/t_0$ , where  $p_e$  is the probability of heralding entanglement, and  $t_0$  is the trial time. The distance between the nodes in the  $L_i - 1$  and in the  $L_i$  is denoted by  $l_0 \cdot a_k^{(n-i)}$ , and  $l_0$  represents the elementary distance between an end node to the first router node. We normalize the rates with  $R$  and the distances with  $l_0$ , and thus they are decoupled from the calculation.

If the memory-photon interfaces are inefficient, or if a network grows by adding more end nodes in a finite area, the routers' insertion loss can dominate the exponential channel losses. In this case, we call dense-node limit, one does not need repeater stations. If operational errors are small enough for the target applications, the total number of qubits across the network is trivial,  $\mathcal{N} \approx 2N \log_k N$ . Thus, the overhead scales as  $\mathcal{N}/N \approx 2 \log_k N$ .

If the network is large and errors accumulate over the target error rate of an application, routers should employ quantum error correction [16]. The code encodes  $n_{\text{phys}}$  qubits into a smaller number of logical qubits  $k_{\text{logic}}$  and can correct up to  $t$  errors ( $[[n_{\text{phys}}, k_{\text{logic}}, 2t + 1]]$  code). Thus,  $n_{\text{phys}}/k_{\text{logic}}$  times more qubits are required to keep the logical entanglement generation rate to be the same as the raw generation rate  $R$ . We consider a subset of CSS codes called "good quantum code" [33] with  $n_{\text{phys}}/k_{\text{logic}} \lesssim 19t$ , saturating Gilbert-Varsharov bound [34]. The encoding exponent, the power of  $t$  in  $n_{\text{phys}}/k_{\text{logic}}$ , of this code is  $J = 1$  resulting in a good scaling. However, other codes can be more suitable for practical considerations such as noise models, connectivities, and device dimensionalities. For this reason, we also consider the surface code with  $n_{\text{phys}}/k_{\text{logic}} = (2t + 1)^2$  ( $J = 2$ ), which demonstrated a high error threshold under circuit noises only with weight-4 stabilizers.

For a given physical error rate  $\epsilon$ , the logical error rate of entanglement swapping is,

$$\epsilon_L \approx (\epsilon/\epsilon_{\text{th}})^t \cdot \epsilon, \quad (1)$$

where  $\epsilon_{\text{th}}$  is the error correction threshold. The expression is based on the statistical argument [35] and works well with topological codes under circuit-level noises. However, any quantum error correction codes satisfying the threshold theorem [34] result in similar scaling. Depending on the code and detailed operations such as decoding, the equation varies by a factor of constant, which we assume one for the simplicity of discussion. We also

exemplify and simplify our calculations with the assumption,  $\epsilon/\epsilon_{\text{th}} = 0.1$ , based on current state-of-the-art hardware [36].

For a dense-node quantum network, the maximum number of entanglement swapping is  $N_{\text{swap}} = 2 \log_k N$ . For a given target error  $\epsilon_0$ ,

$$\epsilon_0 \approx N_{\text{swap}} \epsilon_L = 2 \log_k N 10^{-t} \epsilon. \quad (2)$$

Assuming  $\epsilon_0 = \epsilon$ ,

$$t \approx \log_{10}(2 \log_k N). \quad (3)$$

Thus, the overhead of error-corrected dense-node network is  $\mathcal{N}_{\text{CSS}}/N \approx 38 \log_{10}(2 \log_k N) \cdot \log_k N$  and  $\mathcal{N}_{\text{S.C.}}/N \approx 8 [\log_{10}(2 \log_k N)]^2 \cdot \log_k N$  for CSS and surface-code encoding, respectively.

On the other hand, if the channel loss is dominated by the propagation loss of photons, which we call sparse-node quantum network, we need to consider the additional cost of repeaters. The number of repeaters depends on the geometric details of the deployment. Considering channel length growth rate  $a_k$  in the previous section, the number of entanglement swap is,

$$N_{\text{swap}} = 2 \frac{a_k^n - 1}{a_k - 1}. \quad (4)$$

Thus, with the same assumption on  $\epsilon$ ,  $\epsilon_{\text{th}}$ , and  $\epsilon_0$  as above,

$$t \approx n \log_{10} a_k, \quad (5)$$

where we assumed  $n \log_{10} a_k \gg \log_{10}[2/(a_k - 1)]$  and  $a_k^n \gg 1$ . As a result, the overhead is,

$$\mathcal{N}/N \approx C_J \cdot N^{\log_k a_k} \cdot (\log_k N)^J, \quad (6)$$

$$\text{CSS: } J = 1, C_1 = 38 \cdot \frac{\log_{10} a_k}{a_k - 1} \quad (7)$$

$$\text{Surface Code: } J = 2, C_2 = 8 \cdot \frac{[\log_{10} a_k]^2}{a_k - 1}. \quad (8)$$

Here, we used the fact that every router layer and repeater layer has the same number of memories,  $2N$ , except the root and end nodes with  $N$ , and we multiplied the error correction overhead with the number of repeater and router layers times 2. Thus, we can decompose the overhead into the routing and repeating overhead,  $\sim N^{\log_k a_k}$ , and the error-correction overhead,  $\sim [\log_k N]^J$ .

All in all, Eq. (6) shows that the minimal overhead scaling is with  $J = 1$ , and  $\mathcal{N}/N \sim \mathcal{O}(N^{\log_k a_k} \cdot \log_k N)$ , and the overhead is sublinear for  $a_k < k$ . This is true for the minimal surface covering ( $a_k^{2D} < \sqrt{k}$ ) and the square-lattice covering ( $a_4^{\text{sq}} = 2$ ) as shown in Appendix C. For example, a quaternary QTN with minimal surface covering shows the sub-square-root scaling overhead,  $\mathcal{N}/N \sim \mathcal{O}(N^{1/4} \log_4 N)$ . Similarly, a square-lattice covering quaternary QTN has  $\mathcal{N}/N \sim \mathcal{O}(\sqrt{N} \log_4 N)$ .

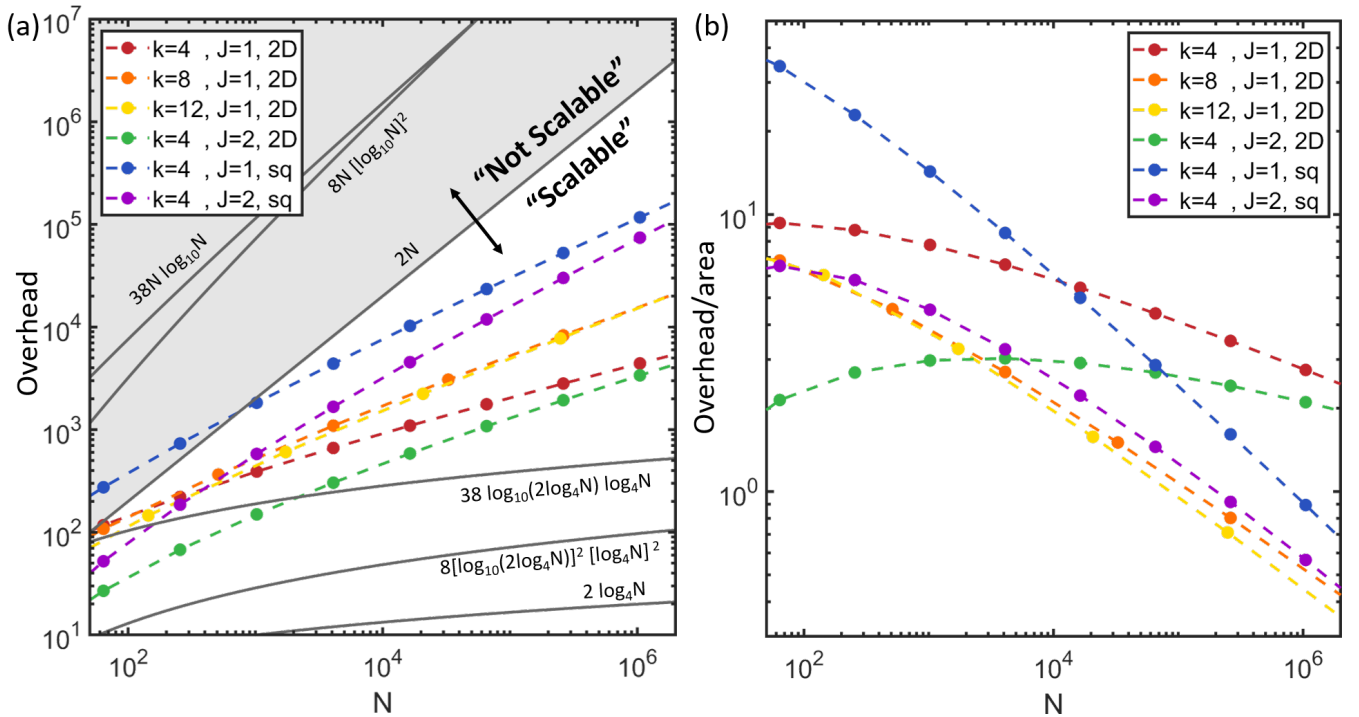


FIG. 2. Resource overhead of QTNs for the user number  $N$  from  $4^3$  to  $4^{10}$ . (a)  $J = 1$ : CSS code encoding,  $J = 2$ : surface code encoding, 2D: minimal surface covering, sq: square-lattice covering. We plot the gray lines for comparison.  $y = 2N$ : boundary of scalable and non-scalable regimes (the factor of 2 from two qubits in entanglement swapping).  $y = 2 \log_4 N$ : non-error-corrected dense-node quantum network with  $k = 4$ .  $y = 38N \log_{10} N$ ,  $8N \log_{10} N$ :  $N$  routing overhead with  $J = 1$  and  $J = 2$  error correction, respectively.  $y = 38 \log_{10}(2 \log_4 N) \log_4 N$ ,  $8[\log_{10}(2 \log_4 N)]^2 [\log_4 N]^2$ : dense-node quantum network with error correction. (b) Area-normalized overheads. We approximate the area as  $\pi(a_k^n l_0)^2$  and  $2(a_k^n l_0)^2$  for minimal surface and square lattice covering.

Figure 2(a) plots the resource overhead of QTNs for the user number  $N$  from  $4^3$  to  $4^{10}$ . The red, orange, and yellow markers show the overhead of  $k = 4, 8, 12$ , CSS-coded ( $J = 1$ ) QTNs deployed to minimally cover the 2D surface (labeled as “2D”). The overhead with surface code encoding ( $J = 2$ ) increases faster (green) but is smaller for  $N \leq 10^6$ . If the network is deployed with square-lattice covering (blue and purple, labeled “sq”), the scaling than the previous. We plot the gray lines for comparison. The line  $y = 2N$  (the factor of 2 comes from the need for entanglement swapping) separates the scalable and non-scalable regimes.  $y = 2 \log_4 N$  line shows non-error-corrected and dense-node QNs for  $k = 4$ . Except for a few, all data points are in the scalable regime between the two lines.  $y = 38N \log_{10} N$  and  $8N \log_{10} N$  lines show the  $N$  routing overhead combined with CSS and surface code error correction, respectively, for a fair comparison with error-corrected QTNs. For  $N \approx 10^6$ , there are five orders of magnitude differences in the overhead.  $y = 38 \log_{10}(2 \log_4 N) \log_4 N$  and  $8[\log_{10}(2 \log_4 N)]^2 [\log_4 N]^2$  lines plot the overhead for dense-node QTN with the two kinds of error correction. Note that all overheads with  $J = 1$  and  $J = 2$  are above the two, respectively.  $k = 4$  QTNs have only  $\approx 10$  (2D, red) and  $\approx 40$  (2D, green) times more overhead than the

minimum, up to  $N \approx 10^6$ .

Figure 2(b) plots the area-normalized overheads in units of qubits/end node/ $l_0^2$  where  $l_0$  is the length of the elementary link. We approximate the area of QTN as  $\pi(a_k^n l_0)^2$  and  $2(a_k^n l_0)^2$  for minimal surface covering and square lattice, respectively. Larger  $k$ -value QTNs (orange and yellow) have a better scaling in  $N$  than the small  $k$  QTN (red). Similarly, the square lattice QTN (blue and purple) scales better than the surface covering QTN (red and green). Small  $k$ , surface-covering QTNs are better for dense nodes — still in sparse-node network limit, where propagation loss dominates the channel loss — while large  $k$ , square lattice QTNs are better for a sparse nodes. For a given distribution of end nodes, one can easily optimize the QTNs with nonuniform branching factors.

## V. NETWORK SIMULATION OF QTN

In the previous Section, we derived the scaling of the overhead in the number of end nodes with uniform random traffic. We did not explicitly consider the balance of the rate at which the end nodes request entanglement and entanglement generation rate. Any network can fail if the

entanglement request rate is too high. In this Section, we simulate a QTN to show that the network is congestion-free below a threshold request rate, and it starts to fail fulfilling the requests after such a threshold. We also analyze the dynamic response of the network to sudden changes in the request rate.

We perform a network-level simulation of the proposed QTN architecture. We developed a discrete-event simulator in Python [37]. The simulation performs a sequence of time cycles of duration  $t_0$ , during which each node attempts entanglement generation. We assume that a successfully generated entanglement lasts 1000 cycles, considering that nitrogen-vacancy (NV) color centers in diamond have a  $10\mu\text{s}$  entanglement trial cycle and an electronic coherence time of 10 ms [11, 19]. In principle, one can extend the coherence time exponentially with error correction. Alternatively, the state can be stored in  $^{13}\text{C}$  nuclear spins with a minute-scale coherence time [38]. For simplicity and network-level study agnostic to physical hardware, we abstract these details and treat entanglement binarily; it only lasts within a coherence time of 1000 cycles and expires regardless of fidelities.

We simulate a  $k = 4$ -ary tree with  $\log_4(N)$  layers. Each node is buffered with  $m = 10$  to support a high rate as well as batched communication. The routers communicate with the rate boosted by the repeater chains, which is aggregated as the same probability of entanglement success. In each cycle, random pairs of clients request entanglement distribution. There are  $n_0 = \binom{N}{2} = N(N-1)/2$  possible communication pairs, each of which randomly requests entanglement with probability  $p_0 = Np/2n_0$  at each cycle. On average,  $Np/2$  requests are created at each cycle, and the probability that a client is in one of the pairs requested is  $\approx p$ . Thus, we call  $p$  the request rate. In the simulation, we sweep  $p_0$  and plot network properties from  $p = 10^{-3}$  to  $p = 10^{-1}$ . We also simulate the network under the batched requests of entanglement with the batch size  $b$ . Each communication pair has a probability  $p_0 = Np/2n_0b$  of a request at each cycle. Although the requests are batched, each request is still completed individually.

A request is fulfilled when all the entanglements along the path between the clients are available. Completing a request depletes them, leaving the memories available for a new entanglement generation. We assume that the time for entanglement swapping is negligible compared to that of entanglement generation. Each node attempts entanglement with the dedicated neighboring nodes (Fig. 1(d)), with a success probability of  $p_e = 0.001$  per trial. Once a qubit is successfully entangled, it remains until the entanglement is consumed, or until it expires after 1000 cycles. When the entanglement expires, the qubits are reset and available for new entanglement. The requests are timed out after 1000 cycles as well. The simulation is repeated and averaged with dynamic sample sizes. At every  $p$ , the simulation was repeated 1000 times or until the 90% confidence interval was smaller

than 1% of the range of possible values, whichever comes first (10 minimum sampling).

In the simulation, we measure the success rate, mean latency, and buffered entanglement. The success rate is the ratio of the number of successfully processed requests to that of all requests. The mean latency is the average cycle of requests. Expired requests contribute to the mean latency with the time out of 1000 cycles. The buffered entanglement is the number of entangled qubit pairs between the router nodes in the network.

Figures 3 (a) and (b) show the success rate and mean latency of requests at a rate from  $p = 10^{-3}$  to  $p = 10^{-1}$  for quaternary QTNs with  $N = 16, 64, 256, 1024$ . We observe the thresholding behavior of the success rate and the mean latency at  $p_{\text{th}} \approx 0.003$ . For  $p \lesssim p_{\text{th}}$ , the success rate approaches unity and the mean latency is negligible. For  $p \gtrsim p_{\text{th}}$ , the network shows increased mean latency, and a fraction of requests expire. It is important that  $p_{\text{th}}$  is independent of  $N$ . Above the threshold, both metrics strongly depend on  $N$  for small  $N$ , but converge to an asymptotic limit for large  $N$ . In the QTN, entanglement flows are bundled as we move up the network hierarchy. This bundling with the routers and repeaters operating first generated first out — in analogy with ‘first-in first-out’ (FIFO) — relaxes the coherence time requirement under probabilistic entanglement generation [27] resulting in the near unity success probability for  $p < p_{\text{th}}$ .

Figure 3 (c) and (d) plot the success rate and mean latency of the batched requests. We fixed a network of size  $N = 256$  and varied the size of the batch  $b$ . For  $b = 2$ , the thresholding behavior remains with a reduced  $p_{\text{th}} \approx 0.002$ . Below the threshold, almost all requests were completed with negligible latencies. The higher the value of  $b$ , the lower the success rates and the higher the mean latencies. Therefore, the curves are smoothed for a large  $b$ . For  $b > m$ , the complete usage of buffered entanglement cannot fulfill the batched requests, and the success rate does not reach near unity for small  $p$ .

Figure 3 (e) shows the dynamic response of  $N = 256$  QTN to the change in request rate ( $b = 1$ ). The rate changes from  $p = 10^{-3}$  to  $p = 10^{-2}$  in time cycle  $10^4$  and reverses back at time cycle  $2 \times 10^4$ . These two values are below and above the threshold, respectively. We repeated the simulation 512 times for averaging and time averaging with discrete time bins of 64 cycles.

After the request rate increased from 0.001 to 0.01 at  $t = 10^3$ , the 90% to 10% fall-time was approximately 1024 cycles for the success rate and 640 cycles for the memory buffer. The 10% to 90% rising time in latency was about 1408 cycles. These changes were slightly offset; the drop in memory buffer came first, followed by a rise in latency, and eventually a fall in success rate as the memory buffer was unable to form enough new entanglements to meet demands. Once the request rate returned to  $10^{-3}$  at  $t = 2 \cdot 10^3$ , the memory buffer immediately began to recover, with a 10% to 90% rising time of approximately 896 cycles. Latency saw a brief spike due to the completion of accumulated requests, which would

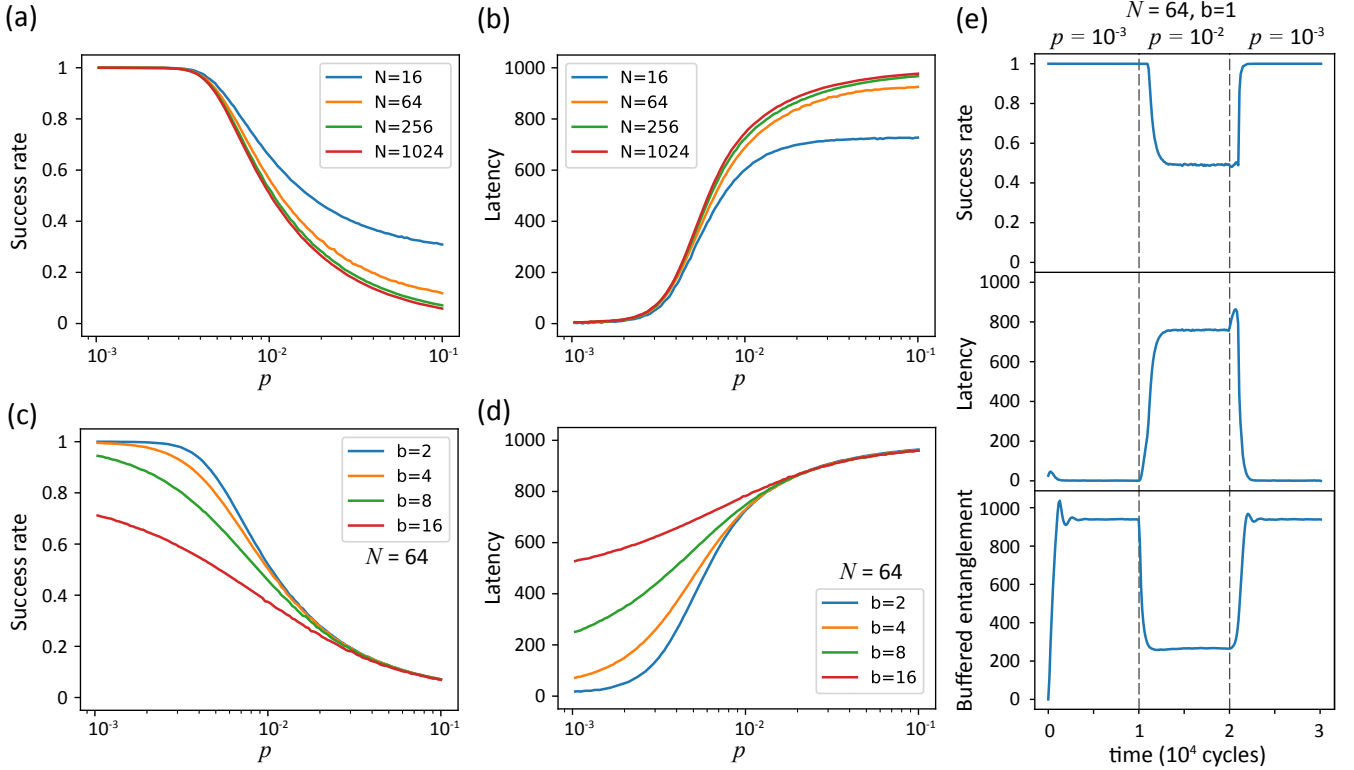


FIG. 3. Characterization of quantum tree network. (a) The success rate of entanglement delivery and (b) mean latency vs.  $p$  for the network sizes of  $N = 4, 64, 256, 1024$ . (c,d) The success rate and mean latency of batched entanglement requests ( $b = 2, 4, 8, 16$ ).  $N = 256$  is used for the network size. Therefore, the thresholding behavior is smoothed for large  $b$ . (a)-(d) The simulation was run repeatedly until the estimate of the mean converged for each data point (see main text). The 90% confidence region of the estimates of the true mean is shaded but is not visible due to small errors. (e) The dynamic responses of QTN. The success rate, the mean latency, and the buffered entanglement of a network ( $N = 256$ ) under a temporary increase in  $p$  from  $10^{-3}$  to  $10^{-2}$  between time cycles of 10,000 and 20,000. 512 simulations were averaged in the ensemble and the values were time-averaged with 64-cycle bins.

have expired over the next few cycles if the network remained busy. During this brief period, the success rate remains low. Once the backlog was processed, latency quickly dropped with a 90% to 10% falling time of 640 cycles, and the success rate abruptly rose, with a 10% to 90% rising time of 256 cycles. Note that these times are measured to the nearest time bucket, which are multiples of 64 cycles. The smaller spike at the beginning of the simulation is because the system starts with no entanglement.

The buffered entanglement exhibited oscillations following sharp increases. This is due to a feedback between entanglement generation and consumption. When there are many entanglements in the network, it is more likely that the entanglements required for any given request will be already present in the buffer. This causes entanglement resources to be consumed faster when the buffer is filled. Meanwhile, entanglement generation attempts occur only between memories that are not already entangled, thus entanglement generation rates are higher when the buffer is empty. This results in the observed os-

cillation until the system reaches an equilibrium in which the entanglement generation rate equals the consumption rate from request fulfillment.

## VI. RESILIENCE AGAINST ATTACKS AND FAILURES

In a targeted attack, an attacker disconnects the network by removing a small fraction of routers [39]. If only a portion of buffered qubits in a router failed, the network continued to operate with reduced performance. However, the tree network topology is vulnerable to router-wise attacks, errors, or other random failures. Each router is only connected to one node in the upper layer, so the removal of a router disconnects the end nodes connected to it from the network.

A possible solution is to have  $q$ -redundant routers that form a Clos network with parent- and child-nodes. In the simplest case where every router is  $q$ -redundant, the total number of qubits increases  $q^2$  times because each of

$q$  routers has  $q$  times the qubits to connect to  $q$  times of upper and lower level routers. Meanwhile, the probability of failure decreases exponentially with  $q$  if router failures are independent. Other hierarchical network structures, in addition to tree networks, can achieve sublinear scaling while offering resilience through redundant pathways.

## VII. CONCLUSION

We introduced the scalability of quantum networks and showed that hierarchical entanglement routing on a quantum tree network is scalable. The overhead of QTNs is logarithmic of the network size if the gate operations are perfect and the channel loss is independent of the layer. The overhead of QTNs with lossy and erroneous channels depends on the deployment. We proposed two scenarios: minimal surface covering and square lattice covering. Incorporating second-generation repeaters for router-to-router routing, we showed that the overhead is  $\mathcal{O}\left(N^{\log_k a_k \log_k N}\right)$ . Furthermore, the quantum tree network does not need time-consuming multipath-finding problems. Our approach is suitable for near-term hardware, including atom-like emitters in diamond [1] or trapped ions [30]. Moreover, the analysis highlights the importance of quantum repeater and router design. Since stochastic behavior normalizes at a larger scale, entanglement routing becomes predictable and readily buffered, improving efficiency and simplifying message passing. Multiplexed architecture with local optical switching is suitable for many memory types (e.g., using photonic circuits, spatial light modulators, and microelectromechanical mirrors).

It is not guaranteed that QTN routing to be optimal; further gains should be possible with locally hierarchical or mesh-tree hybrid graphs. For example, redundant router architecture locally resembling Clos network is discussed to improve the resilience under failures.

By combining low error correction overhead, scalability, and compatibility with classical telecom networks as well as near-term realistic hardware, the hierarchical routing and quantum tree network introduced here present a realistic blueprint to help guide quantum network architectures, protocols, and hardware development.

## ACKNOWLEDGEMENT

We thank Yongshan Ding, Saikat Guha, Hassan Shapourian, Alireza Shabani, Stephen DiAdamo, Siddardha Chelluri, Peter van Loock, and Don Towsley for fruitful discussions. This work was partially supported by AFOSR grant FA9550-20-1-0105 supervised by Gernot Pomrenke, the NSF Center for Quantum Networks (CQN, 1941583), and Cisco Research. H.C. and D.E. acknowledge HSBC, Makena Metcalf, Zapata Computing, and Yudong Cao for MIT QSEC collaboration. H.C. acknowledges the Claude E. Shannon Fellowship and the Samsung Scholarship. M.G.D. acknowledges the DOE CSGF Fellowship.

H.C. and M.G.D contributed equally to this work.

## AUTHOR CONTRIBUTION

D.E. initiated the idea of incompressible entanglement flow in a quantum network. D.E. and H.C. conceived the design of the quantum fat-tree network. H.C. designed and M.G.D. performed the network simulation. H.C. and A.G.I. studied the network congestion and scaling of the network. H.C. studied the scalability of the quantum networks and derived the overheads. A.G.I. studied the vulnerabilities and redundant protection. All authors provided critical feedback and helped shape the research, analysis, and manuscript.

- 
- [1] M. Ruf, N. H. Wan, H. Choi, D. Englund, and R. Hanson, *Journal of Applied Physics* **130**, 070901 (2021).
  - [2] H. J. Kimble, *Nature* **453**, 1023 (2008).
  - [3] P. Arrighi and L. Salvail, *International Journal of Quantum Information* **4**, 883 (2006).
  - [4] Z. Zhang and Q. Zhuang, *Quantum Science and Technology* **6**, 043001 (2021).
  - [5] F. Hahn, A. Pappa, and J. Eisert, *npj Quantum Information* **5**, 1 (2019).
  - [6] M. Hayashi, K. Iwama, H. Nishimura, R. Raymond, and S. Yamashita, in *STACS 2007: 24th Annual Symposium on Theoretical Aspects of Computer Science, Aachen, Germany, February 22-24, 2007. Proceedings 24* (Springer, 2007) pp. 610–621.
  - [7] M. Pant, H. Krovi, D. Towsley, L. Tassiulas, L. Jiang, P. Basu, D. Englund, and S. Guha, *npj Quantum Information* **5**, 1 (2019).
  - [8] A. Patil, M. Pant, D. Englund, D. Towsley, and S. Guha, *npj Quantum Information* **8**, 1 (2022).
  - [9] T. Hasegawa, Y. Tamura, H. Sakuma, Y. Kawaguchi, Y. Yamamoto, and Y. Koyano, *SEI Tech. Rev* **86**, 18 (2018).
  - [10] T. Rudolph, *APL photonics* **2**, 030901 (2017).
  - [11] P. C. Humphreys, N. Kalb, J. P. Morits, R. N. Schouten, R. F. Vermeulen, D. J. Twitchen, M. Markham, and R. Hanson, *Nature* **558**, 268 (2018).
  - [12] H.-J. Briegel, W. Dür, J. I. Cirac, and P. Zoller, *Physical Review Letters* **81**, 5932 (1998).
  - [13] S. D. Barrett and P. Kok, *Physical Review A* **71**, 060310 (2005).
  - [14] H. Bernien, B. Hensen, W. Pfaff, G. Koolstra, M. S. Blok, L. Robledo, T. H. Taminiau, M. Markham, D. J. Twitchen, L. Childress, *et al.*, *Nature* **497**, 86 (2013).

- [15] C. H. Bennett, G. Brassard, S. Popescu, B. Schumacher, J. A. Smolin, and W. K. Wootters, *Physical review letters* **76**, 722 (1996).
- [16] L. Jiang, J. M. Taylor, K. Nemoto, W. J. Munro, R. Van Meter, and M. D. Lukin, *Physical Review A* **79**, 032325 (2009).
- [17] W. J. Munro, A. M. Stephens, S. J. Devitt, K. A. Harrison, and K. Nemoto, *Nature Photonics* **6**, 777 (2012).
- [18] L. G. Roberts, *Proceedings of the IEEE* **66**, 1307 (1978).
- [19] M. Pompili, S. L. N. Hermans, S. Baier, H. K. C. Beukers, P. C. Humphreys, R. N. Schouten, R. F. L. Vermeulen, M. J. Tiggeleman, L. dos Santos Martins, B. Dirkse, S. Wehner, and R. Hanson, *Science* **372**, 259 (2021).
- [20] J. Chow, O. Dial, and J. Gambetta, *IBM Research Blog* (2021).
- [21] M. Zahidy, M. T. Mikkelsen, R. Müller, B. Da Lio, M. Krehbiel, Y. Wang, M. Galili, S. Forchhammer, P. Lodahl, L. K. Oxenløwe, *et al.*, *arXiv preprint arXiv:2301.09399* (2023).
- [22] S. Muralidharan, L. Li, J. Kim, N. Lütkenhaus, M. D. Lukin, and L. Jiang, *Scientific reports* **6**, 20463 (2016).
- [23] G. Vardoyan, S. Guha, P. Nain, and D. Towsley, *ACM SIGMETRICS Performance Evaluation Review* **47**, 27 (2019).
- [24] H. Choi, M. Pant, S. Guha, and D. Englund, *npj Quantum Information* **5**, 104 (2019).
- [25] C. E. Leiserson, *IEEE transactions on Computers* **100**, 892 (1985).
- [26] M. Al-Fares, A. Loukissas, and A. Vahdat, *ACM SIGCOMM computer communication review* **38**, 63 (2008).
- [27] Y. Lee, E. Bersin, A. Dahlberg, S. Wehner, and D. Englund, *npj Quantum Information* **8**, 1 (2022).
- [28] S. C. Benjamin, D. E. Browne, J. Fitzsimons, and J. J. Morton, *New Journal of Physics* **8**, 141 (2006).
- [29] C. Monroe, R. Raussendorf, A. Ruthven, K. R. Brown, P. Maunz, L.-M. Duan, and J. Kim, *Physical Review A* **89**, 022317 (2014).
- [30] K. R. Brown, J. Kim, and C. Monroe, *npj Quantum Information* **2**, 1 (2016).
- [31] N. H. Wan, T.-J. Lu, K. C. Chen, M. P. Walsh, M. E. Trusheim, L. De Santis, E. A. Bersin, I. B. Harris, S. L. Mouradian, I. R. Christen, *et al.*, *Nature* **583**, 226 (2020).
- [32] L. Li, L. De Santis, I. Harris, K. Chen, Y. Song, I. Christen, M. Trusheim, C. E. Herranz, R. Han, and D. Englund, in *2022 Conference on Lasers and Electro-Optics (CLEO)* (IEEE, 2022) pp. 1–2.
- [33] A. R. Calderbank and P. W. Shor, *Physical Review A* **54**, 1098 (1996).
- [34] M. A. Nielsen and I. Chuang, *Quantum computation and quantum information* (2002).
- [35] A. G. Fowler, M. Mariantoni, J. M. Martinis, and A. N. Cleland, *Physical Review A* **86**, 032324 (2012).
- [36] F. Arute, K. Arya, R. Babbush, D. Bacon, J. C. Bardin, R. Barends, R. Biswas, S. Boixo, F. G. Brandao, D. A. Buell, *et al.*, *Nature* **574**, 505 (2019).
- [37] M. Davis, H. Choi, Á. Iñesta G, and D. Englund, quantum tree network, [https://github.com/WolfLink/tree\\_sim](https://github.com/WolfLink/tree_sim) (2023).
- [38] C. E. Bradley, J. Randall, M. H. Abobeih, R. Berrevoets, M. Degen, M. A. Bakker, M. Markham, D. Twitchen, and T. H. Taminiau, *Physical Review X* **9**, 031045 (2019).
- [39] D. Magoni, *IEEE Journal on Selected Areas in Communications* **21**, 949 (2003).
- [40] R. Kershner, *American Journal of mathematics* **61**, 665 (1939).
- [41] E. Friedman, Circles covering circles, <https://erich-friedman.github.io/packing/circovcir/>, accessed: 2023-06-10.
- [42] M. L. Fredman and R. E. Tarjan, *Journal of the ACM (JACM)* **34**, 596 (1987).
- [43] M. Thorup, *SIAM Journal on Computing* **30**, 86 (2000).

## A. CONGESTION IN MESH NETWORK

In this appendix, we investigate congestion in mesh networks. We consider a continuous plane,  $(x, y) \in [0, 1]^2$ , where the points are nodes, and the straight lines by two endpoints are the routing paths. This setting generalizes any uniform lattice to the coarse-graining and renormalization group. To represent uniform random traffic, we randomly choose pairs of points, and the lines defined by a pair are the routing path of entanglement. Note that our following arguments also apply to other mesh networks that are not based on uniform lattices, by adjusting the probability density of choosing points in the plane.

If two routing paths intersect, the point of intersection needs at least a pair of quantum memories for entanglement swapping. Depending on the details of the intersection and the lattice, multiple additional pairs can be required. For example, if two lines intersect with a small angle in a coarse-grained space of a square lattice, the lines share multiple nodes in the original lattice. In the following, we consider the scaling of the number of intersections in the coarse-grained space, and the number of additional memories is lower-bounded by the number of intersections.

Figure 4(a) shows the density map of the intersections made by the  $N_e = 2,000$  lines. Each density in the  $10 \times 10$  grid is normalized with the total number of intersections in the space. The center area has a higher density of intersections. As we will confirm later, the area of high density is independent of  $N_e$ . In a mesh network, the density of intersections is not smooth in a finer grid (Fig. 4(b),  $50 \times 50$  grid). The number of intersections is  $4.3 \times 10^5 \gg 50^2$ , and the fluctuation of density across the grid is not caused by discretization. There is a fluctuation of densities across instances, as shown by comparing Fig. 4(b) and (c). Because of the fluctuation, one needs to buffer each node with enough quantum memories to avoid congestion in the worst case (see main text). Note that the worst-case for each node is still in the typical set of the set of routing paths over a mesh network.

Figure 4(d) plots the number of intersections for different numbers of route paths,  $N_e$ . Each point is the average of 1,000 instances, and the error bars show one standard deviation of the samples ( $\pm\sigma$ ). The black dashed line fits the

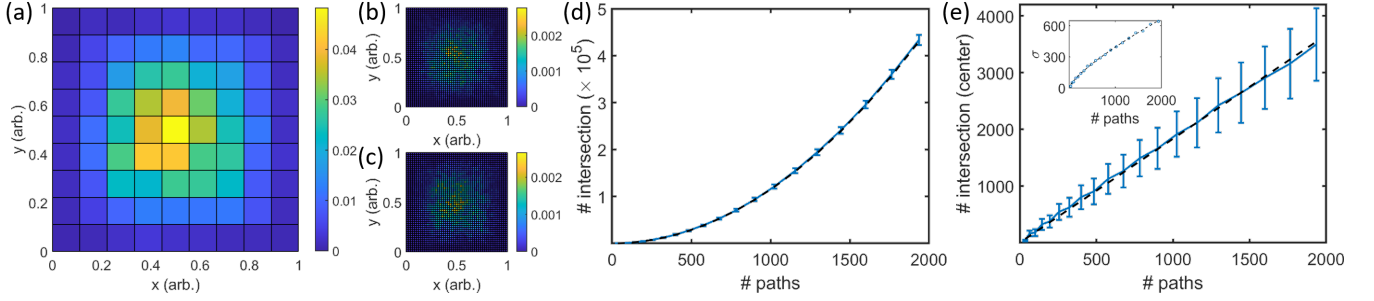


FIG. 4. Congestion of routing paths in a continuous space. (a) Density map of intersections made by  $N_e = 2,000$  routing paths. (b), (c) The instances of density of intersections in a finer  $50 \times 50$  grid. (d) The number of intersections plotted for  $N_e$  paths. Each point is the average of 1,000 instances with one standard device error bar ( $\pm\sigma$ ). Dashed line:  $0.115N_e^2$ . (e) The number of intersections per node is proportional to  $N_e$  ( $\approx 1.832N_e$ ). The inset shows the standard deviations, which grow as  $2.109N_e^{0.757}$ .

router	kind	example pair		probability*
$Nx_0x_1\dots x_y$	branch	$Nx_0x_1\dots x_y\dots x_n$	$Nx_0\dots x'_i\dots x''_{y+1}\dots x''_n$	$(1 - p_{k,y}^2) \cdot p_{k,y} \approx 2k^{-y}$
	root		$Nx_0x_1\dots x_yx'_yx''_{y+1}\dots x''_n$	$(\frac{1}{k})^{2y} \cdot (\frac{k-1}{k})$

\*two  $k$ -ary number of length  $y$  to be different:  $p_{k,y} = 1 - (\frac{1}{k})^y$ , “ $\approx$ ” for  $p_{k,y} \approx 1$ .

TABLE I. Activation Probability of  $y + 1^{\text{th}}$  layer router

data points with  $0.115N_e^2$ . Thus, we confirm that the number of intersections in a mesh network increases as  $\mathcal{O}(N_e^2)$ , and  $\sim \mathcal{O}(N^2)$  if  $N_e \sim \mathcal{O}(N)$ .

Moreover, we investigated the number of intersections in the area that are inversely proportional to  $N_e$ . Assuming  $N_e \sim \mathcal{O}(N)$ , the number of intersections represents the number of intersections per node. Figure 4(e) plots it at the center of  $\sqrt{N_e}/2 \times \sqrt{N_e}/2$  grid with  $\pm\sigma$  error bars. We fit the data points with the black dashed line,  $y = 1.832N_e$  confirming that the intersection per node scales linearly with the number of routing paths. The inset plots the standard deviation of the number of intersections, which grows as  $2.109N_e^{0.757}$ .

## B. ACTIVATION PROBABILITIES

Here, we calculate the activation probability of quantum routers in QTNs. The activation probability of a router is the probability that it needs to perform entanglement swapping for satisfying a communication request. Let us consider the uniform random traffic model where a randomly chosen one of  $N$  end nodes requests for communication with one of  $N - 1$  the others. This is equivalent to randomly choosing a pair out of all possible pairs. Table I shows the activation probability of a router labeled as  $Nx_0\dots x_y$ . The probability that the router is on the routing path, but it is not the highest-layer router on the routing path, is  $(1 - p_{k,y}^2) \cdot p_{k,y}$  (“branch”), where  $p_{k,y} = 1 - (\frac{1}{k})^y$  is the probability that two random  $k$ -ary number of length  $y$  is different. On the other hand, the probability that a router is at the highest level of the routing path (“root”) is  $k^{-2y} \cdot (k - 1)/k$ . The activation probability is the sum of two contributions, and  $\approx 2k^{-y}$  for a large  $k$  or a large  $y$  ( $p_{k,y} \approx 1$ ). Thus, we can expect that the QTN will be congestion-free if the router has exponentially more qubits on the upper layers. Because the number of routers in the upper layer is exponentially smaller, the total number of qubits in each layer will be the same (Fig. 1(d)).

## C. 2D SURFACE COVERING WITH TREE NETWORK

One can question whether the QTN can fully cover the 2D surface to service the user. As an example, let us consider a  $k$ -ary uniform tree. We start from the end node with the area of service enclosed by the circle. The nodes connected to a router should cover the area dedicated to the router, also enclosed by a larger circle. The same process repeats to the higher layer’s router, and the problem maps to the minimal disk covering problem [40]. Figure 5(a) show the  $k = 7$  disk covering problem. The disk covering problem asks for determining the maximum radius of a

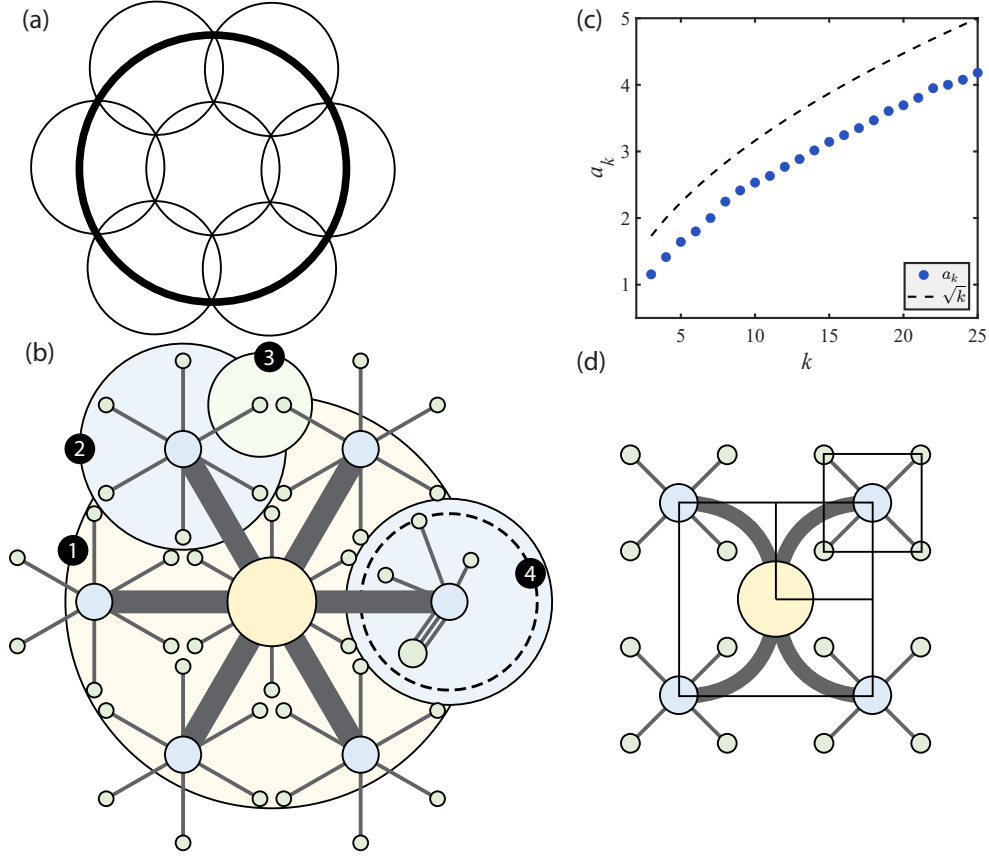


FIG. 5. (a) Optimal solution to the disk covering problem for  $k=7$ . (b) The layout of nodes in a QTN with  $k = 7$  and  $n = 2$ , for a total of  $N = 49$ . Note that there is a blue layer 2 node underneath the center layer-1 node, and there is a green client node under each of the blue layer-2 nodes. (c) A plot of the values of  $a_k$  for various values of  $k$  based on the disk covering problem. (d) A potential layout of a QTN with the end nodes organized in a grid layout. For this layout,  $a_4^{\text{sq}} = 2$ , as demonstrated by the overlaid squares.

circle, of which area is covered by smaller  $k$  circles of unit length. The solution to the minimal disk covering problems is analytically derived for some  $k$ , and numerically known for others [41].

Figure 5(b) shows the application of the problem to QTNs.  $k = 7$  children nodes are spawned from the parent node across the tree. The green end nodes are the children of blue router nodes, and the blue router nodes are the children of yellow router nodes. Furthermore, the yellow nodes can be a child of an upper-layer router. The children are dispersed to cover the coverage of the parent node (①). One green (blue) node is not visible due to overlap with the blue (yellow). The coverage assigned to the blue node (②) is covered by the green nodes (③). If network demands are highly concentrated in a local area, the nodes and the edges can be enhanced with multiplicities (④). Note that the green nodes are not on the blue circle but are slightly inside the circle (④). This is the same for the higher layer nodes, and the blue nodes are inside the yellow circle. The growth rate ( $a_k$ ), the ratio of the blue-green channel length to the green-yellow, is the same as the ratio of green and blue coverage circles.

Figure 5(c) plots  $a_k$  for different  $k$ s. As shown in the plot,  $a_k$  slowly grows with  $k$  and is always smaller than  $\sqrt{k}$ . The dashed line,  $y = \sqrt{k}$ , clearly shows this. One can easily prove  $a_k < \sqrt{k}$ ; the large circle cannot have a larger area than the sum of the  $k$  circle's area;  $\pi(a_k)^2 < k \cdot \pi(1)^2 \rightarrow a_k < \sqrt{k}$ . This guarantees the sub-square-root overhead of QTNs for any  $k$ .

We call the aforementioned construction “minimal surface covering” in the main text, and used  $a_k^{2D}$  for the growth rate. On the other hand, one can consider uniformly locating the end nodes at the positions of vertices of a square lattice. Figure 5(d) shows the deployed nodes as well as channels. The child nodes do not minimally cover the coverage of the parent. An end node covers the square area, on which the points have the node as the nearest one, and the routers are symmetrically dispersed to connect the end nodes with a quaternary tree. We call this “square lattice” construction, with  $a_4^{\text{sq}} = 2$ . Note that  $a_4^{\text{sq}} \neq a_4^{2D} = \sqrt{2}$ .

#### D. RESOURCE OVERHEAD WITH NESTED ERROR CORRECTION

For a  $r$ -nested error correction, each of which can correct upto  $t$  errors, we can derive the logical error rate through induction;

$$\epsilon_L^{(r)} = \epsilon_{\text{th}} \cdot \left( \frac{\epsilon}{\epsilon_{\text{th}}} \right)^{(t+1)^r}. \quad (9)$$

$$t \approx \sqrt[r]{\frac{n \log a_k + \log(\epsilon/\epsilon_0)}{\log(\epsilon_{\text{th}}/\epsilon)} + 1} - 1. \quad (10)$$

Equation (10) recovers Eq. (5) for  $r = 1$ . We can further simplify assuming  $n \log a_k \gg 1$ . Moreover, we assume  $\epsilon = 0.1\epsilon_{\text{th}}$  as the main text. Then,

$$t \approx \sqrt[r]{0.43n \log a_k}. \quad (11)$$

The total number of qubits on the network is,

$$\mathcal{N} = 2f(\mathcal{C}, J, r, t) \cdot N \cdot (a_k^n - 1)/(a_k - 1), \quad (12)$$

where  $f(\mathcal{C}, J, r, t)$  is the encoding rate (physical qubits per logical qubit) and is a function of error correction code  $\mathcal{C}$ , nesting level  $r$ , and the code distance  $2t + 1$ . Assuming Gilbert-Varsharov bound-saturating code at each nesting level,

$$\mathcal{N} \approx 0.86 \frac{\log a_k}{a_k - 1} \cdot 19^r \cdot N^{1+\log_k a_k} \cdot \log_k N. \quad (13)$$

Note that it reconstructs Eq. 6 for  $r = 1$ . This is in contrast to the result that the error correction overhead scales with  $[\log(\text{distance})]^r$  shown in [16]. We attributed this discrepancy to our error normalization. We decide  $t$  changing  $r$  for a fixed target error rate ( $\epsilon_0$ ), while Jiang et. al. fixed  $t$  increasing  $r$  for a lower error rate [16]. There can be an alternative situation where physical constraints limit the maximum  $t = t_{\text{max}}$ , e.g. by a maximum weight of stabilizers, and a larger distance communication at a fixed error rate is only achieved by increasing  $r$ . In this case,

$$r \approx \log \left( \frac{\log(\text{distance})}{\log(\epsilon_{\text{th}}/\epsilon)} \right) / (t + 1). \quad (14)$$

$$\mathcal{N} \propto \text{distance} \cdot [\log(\text{distance})]^{2.94} \quad (15)$$

where  $2.94 = \log 19$  is from the encoding rate  $n_{\text{phys}} \approx 19t$ .

Table II summarizes the comparison.

$t$	$r$	error normalization	scaling	note
variable	1	✓	$\log L$	Eq. (6)
variable	variable	✓	$19^r \cdot \log L$	Eq. (13)
fixed	variable	✗	$[\log L]^r$	Ref. [16]
$t_{\text{max}}$	variable	✓	$[\log L]^{2.94}$	Eq. (15)

TABLE II. Cost coefficient scaling on distances ( $L$ : total distance)

#### E. RESOURCE OVERHEAD WITH ROUTER-ROUTER ENCODING

In this section, we reverse the layer labeling and use  $I = n - i \in 0, 1, \dots, n$ , i.e. end nodes are in  $I = 0^{\text{th}}$  layer.  $I^{\text{th}}$ -layer routers route entanglement from  $k^I$  end nodes, and the raw entanglement generation rate required between the  $I^{\text{th}}$  and  $(I + 1)^{\text{th}}$  layers is  $\sim k^I \cdot R$ . The number of router stations at the  $I^{\text{th}}$  layer is  $N/k^I$ , and the number of qubits in the repeater chain between the  $I^{\text{th}}$  and  $(I + 1)^{\text{th}}$  layers is  $\sim 2a_k^I \cdot k^I \cdot \text{Poly}[\log(a_k^I)]$  (a factor of 2 comes from the two sides). Taking into account the total number of physical qubits in the interval  $[I, I + 1)$ , we have

$\sim 2CN \cdot [\log(a_k)]^J \cdot a_k^I I^J = C' N a_k^I I^J$ , where  $J$  is the exponent of the encoding rate,  $C$  is the constant (see Appendix D), and  $C'(a_k, J) = 2C [\log(a_k)]^J$ . Taking into account the entire network, we find that the number of qubits is  $\mathcal{N} \approx C' N \sum_{I=0}^{n-1} (a_k^I I^J) = C' N (\text{Li}_{-J}(a_k) - a_k^n \Phi(a_k, -J, n))$ , where  $\Phi$  denotes the Lerch transcendent, and  $\text{Li}_s(z)$  is the Jonquiere function with complex order  $s$  continued analytically to  $z > 1$ . We can approximate and simplify transcendent functions;  $\mathcal{N} < C' N (\sum_{I=0}^{n-1} a_k^I) \cdot (\sum_{I=0}^{n-1} I^J) < C'' N \cdot a_k^n \cdot H_{n-1}^{(-J)} \approx C'' N^{1+\log_k(a_k)} \cdot (\log_k N)^{J+1} / (J+1)$ , where  $H_n^{(-J)}$  is the generalized harmonic number of order  $-J$ , and  $C'' = C' / (a_k - 1)$ .

## F. MULTIPATH FINDING

A central challenge in operating a networked quantum system with probabilistic links is that it requires the nodes to hold the memory until the end of the communication of the end nodes. This raises the problem of efficient multipath findings within short communication and computation times. Finding and maximizing the number of independent paths on a graph with probabilistic edges, for a set of randomly generated requests, is challenging. Firstly, the computation requires global knowledge of the network, meaning that routers cannot make routing decisions without waiting for information from other nodes. Secondly, the time complexity of finding paths grows super-linearly with the size of the graph. The specific time complexity depends on the characteristics of the graph itself and can vary. For more information on the time complexity of different graph types, refer to [7, 42, 43].